

Generation of a single-cycle surface acoustic wave pulse on LiNbO_3 for application to thin film materials

Koji Fujiwara,¹ Shunsuke Ota,^{2,3} Tetsuo Kodera,² Yuma Okazaki,³ Nobu-Hisa Kaneko,³ Nan Jiang,^{1,4,5} Yasuhiro Niimi,^{1,4,5} and Shintaro Takada^{1,4,5,6}

¹*Department of Physics, Graduate School of Science, Osaka University, Toyonaka, Osaka 560-0043, Japan*

²*Department of Electrical and Electronic Engineering, Institute of Science Tokyo, Meguro-ku, Tokyo 152-8552, Japan*

³*National Metrology Institute of Japan (NMIJ), National Institute of Advanced Industrial Science and Technology (AIST), Tsukuba, Ibaraki 305-8563, Japan*

⁴*Center for Spintronics Research Network, Osaka University, Toyonaka, Osaka 560-8531, Japan*

⁵*Institute for Open and Transdisciplinary Research Initiatives, Osaka University, Osaka 565-0871, Japan*

⁶*Center for Quantum Information and Quantum Biology (QIQB), Osaka University, Osaka 565-0871, Japan*

(*Electronic mail: takada@phys.sci.osaka-u.ac.jp)

(Dated: 4 July 2025)

Surface acoustic wave (SAW) technology has been explored in thin-film materials to discover fundamental phenomena and to investigate their physical properties. It is used to excite and manipulate quasi-particles such as phonons or magnons, and can dynamically modulate the properties of the materials. In the field, SAWs are typically excited by a continuous wave at a resonant frequency. Recently, generation of a single-cycle SAW pulse has been demonstrated on GaAs substrate. Such a SAW pulse provides a potential to access a single quasi-particle excitation and to investigate its dynamics by time-resolved measurements. On the other hand, to modulate and control the properties of thin film materials, it is generally required to generate high-intensity SAWs. In this work, we demonstrate the efficient generation of a SAW pulse using a chirp interdigital transducer (IDT) on LiNbO_3 substrate. We have fabricated chirp IDT devices with bandwidths from 0.5 GHz to 5.5 GHz. We also confirmed the generation of a SAW pulse with 0.3 ns FWHM (full width at half maximum) by performing time-resolved measurements. The conversion efficiency between input power and SAW on LiNbO_3 substrate is approximately 45 times larger than that on GaAs substrate. This enables us to generate a high-intensity SAW pulse, meeting the requirement for the modulation of thin films. Our results will expand the research in the field, such as spintronics and magnonics, and lead to their further advancements.

Surface acoustic waves (SAWs) are sound waves that propagate along solid surfaces. SAW-based technologies are utilized in many electronic devices, such as microwave bandpass filters and various sensors for detecting pressure, temperature, and chemical vapors, among others. SAWs have also found applications in various fields of fundamental research, including superconducting quantum circuits, semiconductor electron systems, and spintronics¹⁻³.

In general, SAWs are electrically generated and detected by using an interdigital transducer (IDT) fabricated on a piezoelectric substrate⁴. Piezoelectric effect converts electrical signals into mechanical vibrations and vice versa. Due to piezoelectric coupling, SAWs transmit both mechanical strain and electric fields. The piezoelectric material is chosen depending on the purpose of the research. GaAs substrate is, for example, employed to demonstrate quantized charge pumping⁵, single-electron transport^{6,7}, exciton transport⁸, or single-photon emission^{9,10}. In these experiments, GaAs substrate is employed since it can host high mobility two-dimensional electron gas. On the other hand, GaAs has a relatively small electromechanical coupling factor K^2 that describes the efficiency of piezoelectric coupling, about 0.07 %.

For more efficient generation and detection of SAWs, LiNbO_3 is a typical choice of a substrate. K^2 of 128° Y-

cut LiNbO_3 is about 5.6 %, which is 80 times larger than GaAs. Over the past decade, thin film materials have been deposited on a LiNbO_3 substrate and electric fields and/or mechanical strain accompanying to SAWs are utilized to modulate their electronic properties^{2,3}. In particular, van der Waals materials¹¹ have been intensively studied and a variety of physics has been investigated¹²⁻¹⁶. SAWs have also been employed in spintronics, where, for example, switching magnetization^{17,18} and generation of spin current^{19,20} or skyrmions²¹ have been reported. In the applications, the amplitude of the modulations induced in the thin films can be lowered compared to the one at the surface of the piezoelectric substrate without any thin films on top. For example, the electric field inside a metallic thin film induced by SAWs reduces several orders of magnitude. As a result, it is critical to employ a piezoelectric substrate with a large K^2 such as LiNbO_3 to efficiently modulate the electronic properties of materials deposited on top.

Typically, a SAW used in the research introduced above is a sinusoidal wave at the resonant frequency of the IDT having a constant periodicity. On the other hand, it is also possible to use, for example, a rectangle or a saw-tooth wave of SAW by employing a proper IDT structure²². SAWs propagate while keeping their shape due to their linear dispersion.

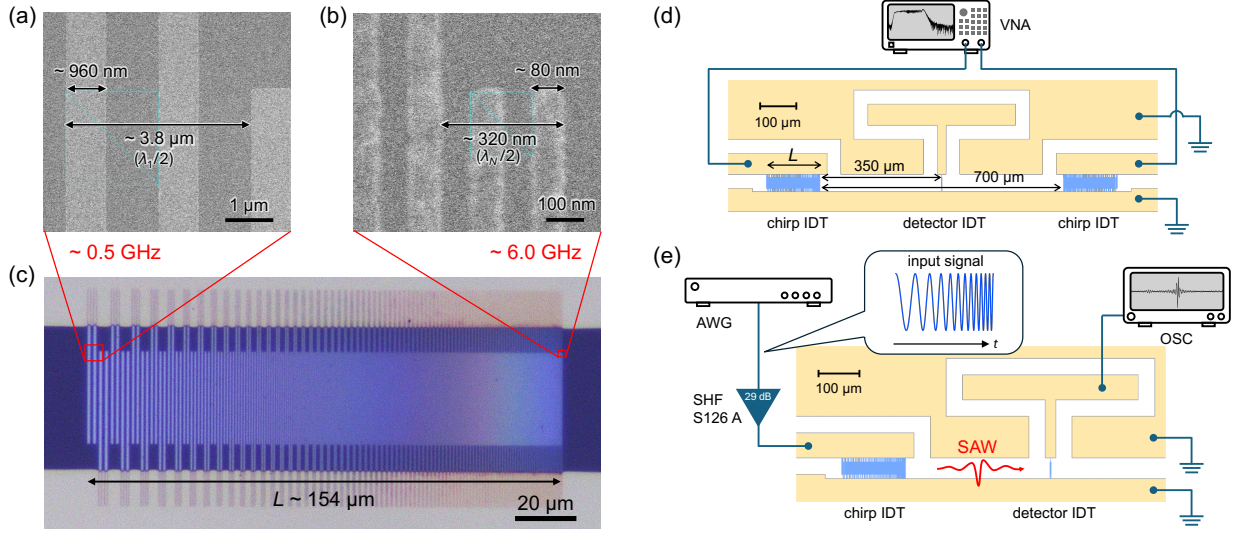


FIG. 1. (a), (b) SEM image of the fabricated chirp IDT. The region zoomed in (a) is for $f_1 \approx 0.5$ GHz SAW excitation and the one in (b) is for $f_N \approx 6.0$ GHz SAW excitation. (c) Optical microscope image of the whole chirp IDT ($T = 40$ ns). The length of the chirp IDT L is given by: $L = T v_{\text{SAW}(\text{design})}$. (d) Schematic illustration of the whole device and setup used in frequency-response measurement between two chirp IDTs. Two chirp IDTs are placed separated by $700 \mu\text{m}$. Their orientations are reversed between left and right. The detector IDT is placed at the middle of the two chirp IDTs. Transmission property is also measured between the chirp IDT and the detector IDT. (e) Schematic illustration of the setup used in time-resolved measurement.

Recently, the generation of a single cycle-SAW pulse has been demonstrated by employing the IDT with a chirped structure, so-called a chirp IDT, on GaAs substrate²³. In the work, the SAW pulse was applied to demonstrate high efficiency single-electron transfer. When the SAW pulse is applied to thin-film materials, it will expand the associated research field and open the possibility, for example, to study the dynamics of SAW induced phenomena. However, as discussed above such applications generally requires high intensity SAWs and hence a substrate having a large K^2 is employed for efficient generation of SAWs. Therefore, it is desirable to demonstrate the generation of a single-cycle SAW pulse on a substrate having a larger K^2 than a GaAs substrate.

In this work, we fabricate chirp IDT devices on 128° Y-cut LiNbO_3 substrate for the application to modulate the electronic properties of thin film materials deposited on top. We measure the frequency response of the devices with different numbers of IDT finger pairs. We, then, demonstrate the generation of a SAW pulse by time-resolved measurements. The amplitude of the SAW signal is expected to increase dramatically compared to GaAs according to high K^2 factor of LiNbO_3 .

SAWs employed to modulate thin-film materials are typically generated by an IDT having a certain number of finger pairs fabricated with a constant period, λ . When the IDT is excited by a continuous radio-frequency signal with a frequency of $f = v_{\text{SAW}}/\lambda$ where v_{SAW} is a velocity of SAWs, SAWs excited from each finger pair constructively interfere. As a result, higher intensity SAWs are generated continuously. Here we employed a chirp IDT²³ to generate a single-cycle SAW pulse. The finger spacing of the chirp IDT gradually

varies from λ_1 to λ_N , allowing each pair of fingers to excite SAWs with different frequencies. By applying an appropriate voltage to the chirp IDT with a frequency varying from f_1 to f_N , SAWs are superposed in the bandwidth from f_1 to f_N . As SAWs have linear dispersion over a wide frequency band, the waveform of the SAW pulse remains unchanged while it propagates. In-phase superposition of SAWs with different frequencies can generate a single-cycle SAW pulse, similar to the generation of a delta function.

When designing a chirp IDT, parameters $v_{\text{SAW}(\text{design})}$, T , f_1 and f_N are determined first. $v_{\text{SAW}(\text{design})}$ is the speed of SAWs in the area of the IDT, T is the time connected to the total spatial length of the IDT as $L = T v_{\text{SAW}(\text{design})}$. f_1 and f_N are the minimum and the maximum frequencies of SAWs generated by the IDT. Here $v_{\text{SAW}(\text{design})} = 3800 \text{ m/s}$ was employed taking into account the damping of SAWs by metal fingers of the IDT. We chose f_1 and f_N to be 0.5 GHz and 3 GHz , where the maximum and the minimum wavelengths of SAWs, $\lambda_n = v_{\text{SAW}(\text{design})}/f_n$, became $7.5 \mu\text{m}$, $1.27 \mu\text{m}$, respectively. The number of finger pairs N was determined by satisfying $\sum_{n=1}^N \lambda_n / v_{\text{SAW}(\text{design})} \approx T$. For $T = 40 \text{ ns}$, N is 56 and L becomes about $154 \mu\text{m}$. We also fabricated chirp IDTs designed with $f_1 = 0.5 \text{ GHz}$ and $f_N = 6.0 \text{ GHz}$ ($\lambda_N \approx 0.63 \mu\text{m}$). In addition, we fabricated a broadband-detector IDT between two chirp IDTs to evaluate the SAW shape. The full width at half maximum (FWHM) of the IDT resonance is given by f_{0d}/N_{pd} , where f_{0d} is the resonant frequency and N_{pd} is a number of finger pairs of the detector IDT. As a result, a smaller N_{pd} enables detection of a wide band SAW signals. In this study, the detector IDTs were designed with $N_{pd} = 1.5$ for all devices, $f_{0d} = 2.5 \text{ GHz}$ ($\lambda_{0d} = 1.52 \mu\text{m}$) for 3 GHz devices

and $f_{0d} = 4.5$ GHz ($\lambda_{0d} = 0.844 \mu\text{m}$) for 6 GHz devices. The length of the aperture was chosen to be $30 \mu\text{m}$ for all the IDTs.

We used open-source Python library “idtpy”²⁴ to design and simulate IDTs. The electrode of IDTs were fabricated using electron-beam lithography with 3 % polymethyl-methacrylate (PMMA) resist. Ti (3 nm) and Al (27 nm) were deposited onto the substrate in a vacuum chamber. We also fabricated the contact pads using laser lithography and Ti (20 nm) and Au (80 nm) were deposited. Scanning electron microscope (SEM) and optical microscope images of a typical chirp IDT device are shown in Figs. 1(a), 1(b) and 1(c). The chirp IDT used in this study adopts a double-finger configuration, as also employed in Ref. 23. Such structures are typically used to suppress acoustic resonance within the IDT^{25,26}.

Figure 1(d) and 1(e) are schematic illustrations of the measurement setup for characterization of frequency response and time-resolved measurement, respectively. We measured the transmission S -parameter (S_{21}) to characterize the frequency response of IDTs using the vector network analyzer (Keysight E5080A). For time-resolved measurement, we used the arbitrary waveform generator (AWG, Keysight M8190A) to apply a chirped signal to a chirp IDT. In order to characterize the shape of SAWs, the sampling oscilloscope (OSC, Keysight N1010A) was connected to a detector IDT. The broadband amplifier (SHF S126 A, 80 kHz - 25 GHz, Gain 29 dB) was inserted between AWG and a chirp IDT to improve the signal-to-noise ratio. In this study, all measurements were performed by a semiautomatic-probe system at room temperature.

Firstly, we measured frequency response between two chirp IDTs to characterize the device properties. The transmission property of the chirp IDTs designed with $T = 40$ ns, $f_N = 3.0$ GHz measured by VNA is shown with the blue line in Fig. 2(a). The result shows that power transmission by SAWs appears from around 0.5 GHz to 3.0 GHz. The average value of $|S_{21}|$ between $f = 0.5$ GHz and 3.0 GHz was -46 dB. This is approximately 30 dB larger than the one on GaAs²³, and hence 32 times higher power conversion efficiency at each chirp IDT is expected. Similar measurements were performed on a device designed with $f_N = 6.0$ GHz and $T = 40$ ns, confirming its operation within the frequency band of 0.5 GHz to 5.5 GHz (Fig. 2(c)). Additionally, to evaluate the characteristics of the detector IDT, the transmission characteristics from one chirp IDT to the detector IDT were also measured (Figs. 2(b) and 2(d)). Simulation responses shown with gray lines were obtained by calculation based on delta-function model using “idtpy”²⁴. The simulated results are in good agreement with the experimental results. The characteristics obtained from this simulation will be used later for reproducing the SAW waveform.

In a chirp IDT on GaAs, it is known that an increase in T enhances the SAW excitation efficiency.²⁷ To investigate the T dependence on a LiNbO₃ substrate, chirp IDTs with different T values were fabricated on the same substrate, and their characteristics were evaluated. $|S_{21}|$ between a pair of chirp IDTs for the devices with various T are shown in Fig. 3(a). When T is increased, transmission signals decreased and some dip structures appeared. We show the average value of $|S_{21}|$ from 0.5 GHz to 3.0 GHz for various T in Fig. 3(b). The ampli-

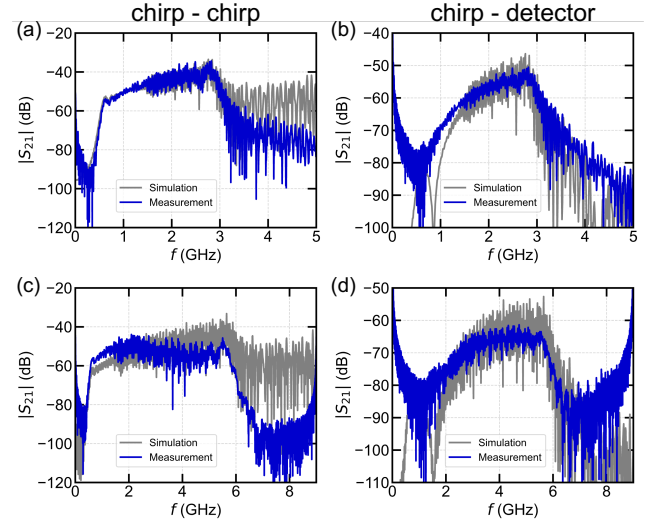


FIG. 2. (a) Transmission property $|S_{21}|$ between a pair of chirp IDTs with $T = 40$ ns, $f_1 = 0.5$ GHz, $f_N = 3.0$ GHz, and $v_{\text{SAW}(\text{design})} = 3800$ m/s. These data were obtained by time-domain gating analysis to exclude electromagnetic crosstalk components. The gray line shows the simulated response of the designed chirp IDT based on delta-function model. (b) Transmission property $|S_{21}|$ between the chirp IDT to the detector IDT with 1.5 pairs of fingers, $f_{0d} = 2.5$ GHz, $v_{\text{SAW}(\text{design})} = 3800$ m/s. The gray line is obtained by convoluting the simulated response of the chirp IDT and the detector IDT. (c), (d) The same datasets as (a), (b) for the devices designed with $f_1 = 0.5$ GHz, $f_N = 6.0$ GHz. The detector IDT is a regular IDT with 1.5 pairs of fingers, $f_{0d} = 4.5$ GHz, $v_{\text{SAW}(\text{design})} = 3800$ m/s.

tude of transmission tends to decrease with increasing of T . We also measured transmission properties between one chirp IDT and the detectors IDT (Figs. 3(c) and 3(d)). As the variation in quality of detector IDT is considered to be relatively small, in this case, the tendency of decrease of $|S_{21}|$ is observed more clearly. A similar behavior was observed for the 5.5 GHz chirp IDT device (Figs. 3(e)–3(h)). This is a different tendency from the one for GaAs²⁷.

One possible reason is that the input power is enclosed in the chirp IDT itself as the electro-mechanical coupling coefficient K^2 of LiNbO₃ is 80 times higher than GaAs. The electromechanical coupling coefficient K^2 is given by $K^2 \propto |(\nu_0 - \nu_m)/\nu_0|$, where ν_0 and ν_m are the SAW velocities when the substrate surface is adjacent to vacuum and an infinitesimally thin perfect conductor, respectively^{28,29}. A high K^2 means a large difference between ν_0 and ν_m . This leads to larger reflections of the SAW at the boundary between the free surface and the metal electrode of IDT fingers. As a result, an increase of the number of fingers will enhance the reflection of SAWs within IDTs more rapidly on LiNbO₃ than on GaAs. Here we comment that this effect is more significant when the width of metal electrode is comparable to or longer than the SAW wavelength. To reduce the influence of the effect we designed the IDTs such that a SAW with a longer wavelength passes through the metal electrodes to generate a SAW with a shorter wavelength (see Fig. 1(c)). In a LiNbO₃ substrate, a similar tendency has also been observed for an

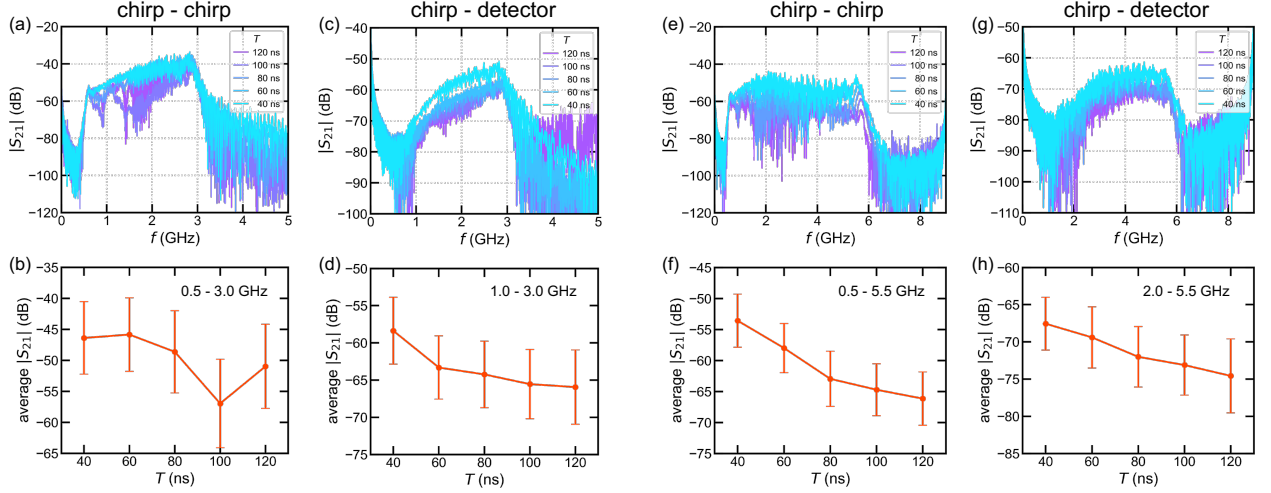


FIG. 3. (a) Transmission property $|S_{21}|$ between two chirp IDTs after time gating. Chirp IDTs with different parameters $T = 40, 60, 80, 100, 120$ ns are compared. These devices are designed with common parameters $f_1 = 0.5$ GHz, $f_N = 3.0$ GHz and $v_{\text{SAW}(\text{design})} = 3800$ m/s. (b) Average of $|S_{21}|$ in the range $f = 0.5$ GHz to $f = 3.0$ GHz for various T . Error bars indicate standard deviation. (c) Transmission property $|S_{21}|$ between chirp IDT to detector IDT after time gating. Detector IDTs are regular IDTs with 1.5 pairs of fingers, $f_{0d} = 2.5$ GHz, $v_{\text{SAW}(\text{design})} = 3800$ m/s. (d) Average of $|S_{21}|$ in the range $f = 1.0$ GHz to $f = 3.0$ GHz for various T . Error bars represent standard deviation. (e)-(h) The same datasets as (a)-(d) for the devices designed with $f_1 = 0.5$ GHz, $f_N = 6.0$ GHz. Detector IDTs are regular IDTs with 1.5 pairs of fingers, $f_{0d} = 4.5$ GHz, $v_{\text{SAW}(\text{design})} = 3800$ m/s. For the time-gated analysis, a time window of 170 ns – 450 ns was used for chirp-to-chirp measurements and 80 ns – 220 ns for chirp-to-detector measurements, applied consistently across all devices at both 3 GHz and 5.5 GHz.

IDT with a single resonant frequency at 4 GHz. The resonant transmission between the IDTs saturates around $T = 50$ ns. For more detailed discussion, further investigation of power confinement effects in chirp IDTs, for example by comparing with narrow-band IDTs of minimal size or by directly measuring surface displacements using optical methods such as laser Doppler vibrometry^{30–33}, would provide valuable insights. In this study, measurements were only conducted with parameters above $T = 40$ ns. To find the optimal condition more investigation within the range of $T < 60$ ns is required.

Next we performed time-resolved measurement using the 3 GHz chirp IDT device designed with $T = 40$ ns, which shows the highest transmission S_{21} from the chirp IDT to the detector IDT (Figs. 3(c) and 3(d)). From the design parameters of the IDT, $v_{\text{SAW}(\text{design})} = 3800$ m/s, $T = 40$ ns, $f_1 = 0.5$ GHz, and $f_N = 3$ GHz, we obtained the waveform of the input signal using “idtpy”²⁴. The input signal was generated by AWG, amplified by the broadband amplifier (29 dB gain), and applied to the chirp IDT. The amplitude of the output signal from AWG was set to $0.4 V_{\text{pp}}$ for all the frequencies. The SAW signal generated by the chirp IDT propagated along the wafer and was converted to the voltage signal by the detector IDT. Then it was measured by using a sampling oscilloscope. In this measurement, it is important to tune the input signal to compensate the mismatch between $v_{\text{SAW}(\text{design})}$ and the actual SAW velocity, and also the imperfection of the IDT fabrication such as the metallization ratio of the IDT fingers. The SAW velocity also depends on temperatures. In this study, all measurements were performed at room temperature. However, when measurements are carried out at low temperatures, the input signal needs to be optimized at each

temperature.

The measured signal is shown in Fig. 4(a). The signal appearing in a shorter time ($t < 40$ ns) represents an electromagnetic crosstalk propagating from the chirp IDT with the speed of light during the SAW excitation. The SAW signal was observed at $t = t_d \approx 128$ ns, where t_d is the flight time of the SAW signal between the chirp IDT and the detector IDT. The measured SAW signal is shown in Fig. 4(b) with the blue line. Here this signal differs from the actual waveform of the SAW due to the finite bandwidth of the detector IDT. The actual waveform can be numerically calculated based on impulse-response model using “idtpy”²⁴. To do that we firstly reproduced the measured signal in the simulation, which is shown with the gray line. After finding the good agreement between the measured signal and the simulation, we subtract the influence of the detector IDT from the simulation, obtaining the actual SAW waveform shown with the red line in Fig. 4. Consequently, a SAW pulse with a FWHM of approximately 0.3 ns was obtained. Its shape represents the time-dependent electric potential of the SAW pulse generated by the chirp IDT. Note that the displacement of the piezoelectric substrate is proportional to the electric potential induced by the SAWs. We also note that our time-resolved measurement detects the average shape of the SAWs over the aperture and is insensitive to the transverse amplitude distribution across the aperture. The transverse amplitude distribution can affect the material property modulations, depending on parameters such as the IDT’s aperture length, SAW wavelength, and the material’s position relative to the IDT. Special IDT designs, such as apodization^{34–36}, are useful for suppressing the transverse amplitude distribution.

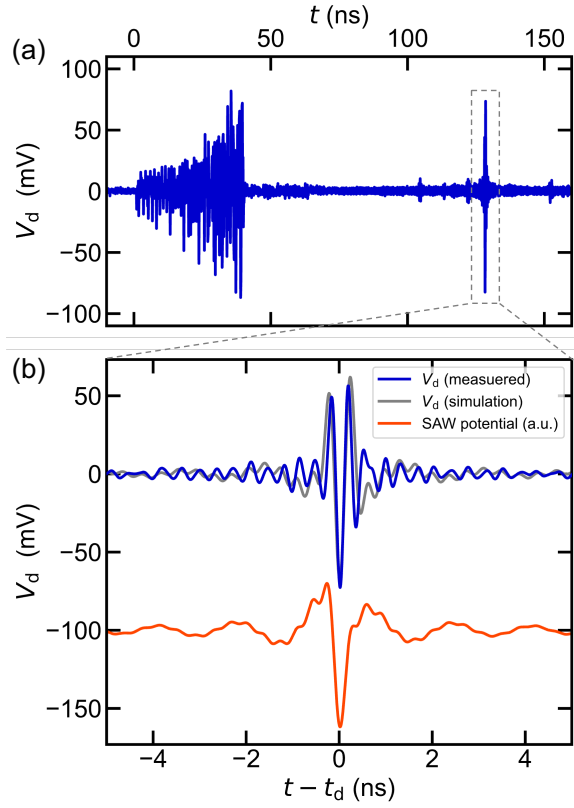


FIG. 4. Time-resolved measurement of a SAW pulse signals for $T = 40$ ns device. (a) Voltage signals detected by the detector IDT. (b) Zoomed-in area of SAW related signals in $t_d \approx 128$ ns. t_d is the flight time of the SAW signal between the chirp IDT and the detector IDT. The blue line indicates the measured data and the gray line is the simulated signal detected by the detector IDT. The red line is SAW electric potential obtained by deconvolving the property of the detector IDT from the simulated signal (arbitrary unit).

The detected voltage amplitude V_d was approximately 130 mV_{pp} (peak to peak). When we compare the power conversion efficiency of this chirp IDT with the similar one ($T = 120$ ns, $f_1 = 0.5$ GHz, $f_N = 3.0$ GHz) on a GaAs substrate in a previous study²⁷, it is 45 times more efficient for the chirp IDT on LiNbO₃. In this study, we focused only on the generation of a single-cycle SAW pulse. A chirp IDT, however, can superimpose frequency components from f_1 to f_N by exciting a waveform with frequency $f(t)$ at a given time t . By appropriately controlling the amplitude and phase of each frequency component, it is possible to excite SAWs with arbitrary waveforms that can be expressed within the frequency band.

In conclusion, we have demonstrated creation of a solitide-SAW pulse on LiNbO₃ substrate. We fabricated chirp IDT devices on a 128°Y-cut LiNbO₃ substrate, ranging from 0.5 to 5.5 GHz. We conducted time-resolved measurement using a chirp IDT with a frequency range of 0.5 GHz–3.0 GHz and $T = 40$ ns, confirming the generation of a SAW pulse with a FWHM of approximately 0.3 ns. From the frequency response of the devices with the different numbers of IDT fin-

ger pairs in the range of $T = 40$ ns to 120 ns, we found that the amplitude of transmission signal decreases when we increase the number of IDT finger pairs. This tendency is in contrast to the similar chirp IDT on GaAs substrate ($f_1 = 0.5$ GHz, $f_N = 3$ GHz), where the amplitude increases while T increases from 40 ns to 120 ns. Nonetheless, with a smaller number of finger pairs the power conversion efficiency of a chirp IDT on LiNbO₃ is 45 times larger than the one on GaAs having more finger pairs.

The efficient generation of the SAW pulse demonstrated in this study will open up possibilities in various thin-film material investigations. In spintronics, for example, generation of pulsed spin current or a single skyrmion, and manipulation of them can be envisioned. Furthermore, combination of the demonstrated efficient SAW pulse generation with thin-film materials makes it possible to modulate the material properties in time-resolved manner. Studying the dynamics of material-property modulations or quasiparticle excitation will expand the research associated with thin-film materials.

This work was supported by JSPS KAKENHI (Grant Nos. JP23H00257, JP22KJ2180) and JST FOREST (Grant No. JP-MJFR2134).

AUTHOR DECLARATIONS

Conflict of Interest

The authors have no conflicts to disclose.

Author Contributions

Koji Fujiwara: Conceptualization (equal); Data curation (lead); Formal analysis (lead); Investigation (lead); Methodology (equal); Software (equal); Validation (equal); Visualization (lead); Writing – original draft (lead); Writing – review & editing (equal). **Shunsuke Ota:** Formal analysis (supporting); Investigation (supporting); Methodology (equal); Software (equal); Writing – review & editing (equal). **Tetsuo Kodera:** Writing – review & editing (equal). **Yuma Okazaki:** Methodology (equal); Writing – review & editing (equal). **Nobu-Hisa Kaneko:** Resources (equal); Writing – review & editing (equal). **Nan Jiang:** Writing – review & editing (equal). **Yasuhiro Niimi:** Conceptualization (equal); Funding acquisition (equal); Resources (equal); Writing – review & editing (equal). **Shintaro Takada:** Conceptualization (equal); Formal analysis (supporting); Funding acquisition (equal); Investigation (supporting); Methodology (equal); Project administration (lead); Resources (equal); Supervision (equal); Software (equal); Supervision (equal); Validation (equal); Visualization (supporting); Writing – original draft (supporting); Writing – review & editing (equal).

DATA AVAILABILITY

The data that support the findings of this study are available from the corresponding author upon request.

REFERENCES

- ¹P. Delsing, A. N. Cleland, M. J. A. Schuetz, J. Knörzer, G. Giedke, J. I. Cirac, K. Srinivasan, M. Wu, K. C. Balram, C. Bäuerle, T. Meunier, C. J. B. Ford, P. V. Santos, E. Cerda-Méndez, H. Wang, H. J. Krenner, E. D. S. Nysten, M. Weiß, G. R. Nash, L. Thevenard, C. Gourdon, P. Rovillain, M. Marangolo, J.-Y. Duquesne, G. Fischerauer, W. Ruile, A. Reiner, B. Paschke, D. Denysenko, D. Volkmer, A. Wixforth, H. Bruus, M. Wiklund, J. Reboud, J. M. Cooper, Y. Fu, M. S. Brugger, F. Rehfeldt, and C. Westerhausen, “The 2019 surface acoustic waves roadmap,” *Journal of Physics D: Applied Physics* **52**, 353001 (2019).
- ²X. Nie, X. Wu, Y. Wang, S. Ban, Z. Lei, J. Yi, Y. Liu, and Y. Liu, “Surface acoustic wave induced phenomena in two-dimensional materials,” *Nanoscale Horiz* **8**, 158–175 (2023), nie, Xuchen Wu, Xiaoyue Wang, Yang Ban, Siyuan Lei, Zhihao Yi, Jiabao Liu, Ying Liu, Yanpeng eng Review England 2022/12/01 *Nanoscale Horiz.* 2023 Jan 30;8(2):158–175. doi: 10.1039/d2nh00458e.
- ³P. Zhao, C. H. Sharma, L. Tiemann, and R. H. Blick, “Surface acoustic wave induced transport and strain phenomena in van der waals materials,” *Journal of Physics D: Applied Physics* **57** (2024), 10.1088/1361-6463/ad3f24.
- ⁴R. M. White and F. W. Voltmer, “Direct piezoelectric coupling to surface elastic waves,” *Applied Physics Letters* **7**, 314 (1965), 72726 Times Cited:736 Cited References Count:6.
- ⁵J. M. Shilton, V. I. Talyanskii, M. Pepper, D. A. Ritchie, J. E. F. Frost, C. J. B. Ford, C. G. Smith, and G. A. C. Jones, “High-frequency single-electron transport in a quasi-one-dimensional gaas channel induced by surface acoustic waves,” *Journal of Physics: Condensed Matter* **8**, L531–L539 (1996), 0953-8984.
- ⁶S. Hermelin, S. Takada, M. Yamamoto, S. Tarucha, A. D. Wieck, L. Saminadayer, C. Bäuerle, and T. Meunier, “Electrons surfing on a sound wave as a platform for quantum optics with flying electrons,” *Nature* **477**, 435–438 (2011).
- ⁷R. P. G. McNeil, M. Kataoka, C. J. B. Ford, C. H. W. Barnes, D. Anderson, G. A. C. Jones, I. Farrer, and D. A. Ritchie, “On-demand single-electron transfer between distant quantum dots,” *Nature* **477**, 439–442 (2011).
- ⁸J. Rudolph, R. Hey, and P. Santos, “Long-range exciton transport by dynamic strain fields in a gaas quantum well,” *Physical Review Letters* **99**, 1–4 (2007), 0031-9007.
- ⁹T.-K. Hsiao, A. Rubino, Y. Chung, S.-K. Son, H. Hou, J. Pedrós, A. Nasir, G. Éthier Majcher, M. J. Stanley, R. T. Phillips, T. A. Mitchell, J. P. Griffiths, I. Farrer, D. A. Ritchie, and C. J. B. Ford, “Single-photon emission from single-electron transport in a saw-driven lateral light-emitting diode,” *Nature Communications* **11**, 917 (2020).
- ¹⁰M. Yuan, K. Biermann, S. Takada, C. Bäuerle, and P. V. Santos, “Remotely pumped ghz antibunched emission from single exciton centers in gaas,” *ACS Photonics* **8**, 758–764 (2021).
- ¹¹K. S. Novoselov, A. K. Geim, S. V. Morozov, D. Jiang, Y. Zhang, S. V. Dubonos, I. V. Grigorieva, and A. A. Firsov, “Electric field effect in atomically thin carbon films,” *Science* **306**, 666–669 (2004).
- ¹²R. Fandan, J. Pedrós, A. Hernández-Minguez, F. Iikawa, P. V. Santos, A. Bosca, and F. Calle, “Dynamic local strain in graphene generated by surface acoustic waves,” *Nano Letters* **20**, 402–409 (2020), pMID: 31790600, <https://doi.org/10.1021/acs.nanolett.9b04085>.
- ¹³M. Yokoi, S. Fujiwara, T. Kawamura, T. Arakawa, K. Aoyama, H. Fukuyama, K. Kobayashi, and Y. Niimi, “Negative resistance state in superconducting nbse2 induced by surface acoustic waves,” *Science Advances* **6** (2020), 10.1126/sciadv.aba1377.
- ¹⁴P. Zhao, C. H. Sharma, R. Liang, C. Glasenapp, L. Mourokh, V. M. Kovalev, P. Huber, M. Prada, L. Tiemann, and R. H. Blick, “Acoustically induced giant synthetic hall voltages in graphene,” *Physical Review Letters* **128** (2022), 10.1103/physrevlett.128.256601.
- ¹⁵Y. Fang, Y. Xu, K. Kang, B. Davaji, K. Watanabe, T. Taniguchi, A. Lal, K. F. Mak, J. Shan, and B. J. Ramshaw, “Quantum oscillations in graphene using surface acoustic wave resonators,” *Physical Review Letters* **130** (2023), 10.1103/physrevlett.130.246201.
- ¹⁶T. P. Lyons, J. Puebla, K. Yamamoto, R. S. Deacon, Y. Hwang, K. Ishibashi, S. Maekawa, and Y. Otani, “Acoustically driven magnon-phonon coupling in a layered antiferromagnet,” *Physical Review Letters* **131** (2023), 10.1103/physrevlett.131.196701.
- ¹⁷S. Davis, A. Baruth, and S. Adenwalla, “Magnetization dynamics triggered by surface acoustic waves,” *Applied Physics Letters* **97** (2010), 10.1063/1.3521289.
- ¹⁸M. Foerster, F. Macia, N. Statuto, S. Finizio, A. Hernandez-Minguez, S. Lendinez, P. V. Santos, J. Fontcuberta, J. M. Hernandez, M. Klau, and L. Aballe, “Direct imaging of delayed magneto-dynamic modes induced by surface acoustic waves,” *Nat Commun* **8**, 407 (2017), foerster, Michael Macia, Ferran Statuto, Nahuel Finizio, Simone Hernandez-Minguez, Alberto Lendinez, Sergi Santos, Paulo V Fontcuberta, Josep Hernandez, Joan Manel Klau, Mathias Aballe, Lucia eng European Research Council/International Research Support, Non-U.S. Gov’t England 2017/09/03 *Nat Commun.* 2017 Sep 1;8(1):407. doi: 10.1038/s41467-017-00456-0.
- ¹⁹M. Weiler, H. Huebl, F. S. Goerg, F. D. Czeschka, R. Gross, and S. T. Goennenwein, “Spin pumping with coherent elastic waves,” *Phys Rev Lett* **108**, 176601 (2012), weiler, M Huebl, H Goerg, F S Czeschka, F D Gross, R Goennenwein, S T B eng 2012/06/12 *Phys Rev Lett.* 2012 Apr 27;108(17):176601. doi: 10.1103/PhysRevLett.108.176601. Epub 2012 Apr 23.
- ²⁰D. Kobayashi, T. Yoshikawa, M. Matsuo, R. Iguchi, S. Maekawa, E. Saitoh, and Y. Nozaki, “Spin current generation using a surface acoustic wave generated via spin-rotation coupling,” *Physical Review Letters* **119** (2017), 10.1103/physrevlett.119.077202.
- ²¹T. Yokouchi, S. Sugimoto, B. Rana, S. Seki, N. Ogawa, S. Kasai, and Y. Otani, “Creation of magnetic skyrmions by surface acoustic waves,” *Nature Nanotechnology* **15**, 361–366 (2020).
- ²²J. R. Schülein/Florian, E. Zallo, P. Atkinson, O. G. Schmidt, R. Trotta, A. Rastelli, A. Wixforth, and H. J. Krenner, “Fourier synthesis of radiofrequency nanomechanical pulses with different shapes,” *Nature Nanotechnology* **10**, 512–516 (2015).
- ²³J. Wang, S. Ota, H. Edlbauer, B. Jadot, P.-A. Mortemousque, A. Richard, Y. Okazaki, S. Nakamura, A. Ludwig, A. D. Wieck, M. Urdampilleta, T. Meunier, T. Kodera, N.-H. Kaneko, S. Takada, and C. Bäuerle, “Generation of a single-cycle acoustic pulse: A scalable solution for transport in single-electron circuits,” *Physical Review X* **12** (2022), 10.1103/physrevx.12.031035.
- ²⁴Junliang-Wang, “Junliang-wang/idtpy: First release,” (2022).
- ²⁵T. Bristol, W. Jones, P. Snow, and W. Smith, “Applications of double electrodes in acoustic surface wave device design,” in *1972 Ultrasonics Symposium* (1972) pp. 343–345.
- ²⁶A. De Vries, R. Miller, and T. Wojcik, “Reflection of a surface wave from three types of id transducers,” in *1972 Ultrasonics Symposium* (1972) pp. 353–358.
- ²⁷S. Ota, *Surface Acoustic Wave-Driven Single-Electron Transport for Quantum Information Processing*, Phd thesis, Tokyo Institute of Technology (2024).
- ²⁸S. Datta, *Surface Acoustic Wave Devices* (Prentice-Hall, 1986).
- ²⁹K. A. Ingebrigtsen, “Surface waves in piezoelectrics,” *Journal of Applied Physics* **40**, 2681–2686 (1969).
- ³⁰J. V. Knuuttila, P. T. Tikka, and M. M. Salomaa, “Scanning michelson interferometer for imaging surface acoustic wave fields,” *Opt Lett* **25**, 613–5 (2000).
- ³¹K. Kokkonen and M. Kaivola, “Scanning heterodyne laser interferometer for phase-sensitive absolute-amplitude measurements of surface vibrations,” *Applied Physics Letters* **92** (2008), 10.1063/1.2840183.
- ³²K. y. Hashimoto, K. Kashiwa, N. Wu, T. Omori, M. Yamaguchi, O. Takano, S. Meguro, and K. Akahane, “A laser probe based on a sagnac interferometer with fast mechanical scan for rf surface and bulk acoustic wave devices,” *IEEE Transactions on Ultrasonics, Ferroelectrics, and Frequency Control* **58**, 187–194 (2011).
- ³³M. Fisicaro, T. A. Steenberg, Y. C. Doedes, K. Heeck, and W. Löffler, “Imaging transverse modes in a gigahertz surface-acoustic-wave cavity,” *Physical Review Applied* **23** (2025), 10.1103/PhysRevApplied.23.014032.

- ³⁴T. Omori, T. Suyama, K. Shimada, A. Chang-Jun, M. Yamaguchi, and K. y. Hashimoto, "Theoretical considerations on suppression mechanism of spurious transverse mode resonances in wideband saw resonators on linbo3," in *2011 IEEE International Ultrasonics Symposium*, pp. 830–834.
- ³⁵Y. Yin, W. Jiang, W. Huang, and A. Gao, "Using crossed idts to suppress transverse modes in saw resonators based on poi substrate," in *2022 IEEE International Ultrasonics Symposium (IUS)*, pp. 1–4.
- ³⁶Y. Guo, M. Kadota, and S. Tanaka, "Suppression of transverse mode on linbo3/ quartz hetero acoustic layer surface acoustic wave resonator by zigzag shape apodization," in *2023 Joint Conference of the European Frequency and Time Forum and IEEE International Frequency Control Symposium (EFTF/IFCS)*, pp. 1–3.